Glass and Ceramics, Vol. 70, Nos. 7 – 8, November, 2013 (Russian Original, Nos. 7 – 8, July – August, 2013)

UDC 666.31

MECHANISM OF LIQUID-PHASE SINTERING OF SILICON CARBIDE AND NITRIDE WITH OXIDE ACTIVATING ADDITIVES

S. N. Perevislov[1]

Translated from *Steklo i Keramika*, No. 7, pp. 34 – 38, July, 2013.

The mechanism of sintering and the particulars of structure formation in liquid-phase-sintered silicon carbide and sintered silicon nitride were studied. The formation of the structure core (SiC or Si_3Ni_4 grains) – boundary layer (SiC oxide or SiAlON) – intergrain phase (oxides) was recorded.

Key words: silicon carbide, silicon nitride, sialon.

Owing to their high strength and hardness, good stability against oxidation and resistance to thermal shock as well possibilities for retaining mechanical properties at high temperatures silicon carbide based ceramic materials are widely used as construction materials in many areas of technology. Silicon carbide belongs to a class of compounds with strong covalent bonds, which impedes mass transfer during sintering without the use of special additives. Ordinarily, dense SiC-ceramic is obtained by means of liquid-phase sintering with oxide additives. The most promising ones are Al_2O_3, Y_2O_3 and MgO, which promote the formation of melt and sintering by the liquid-phase method during heat-treatment [1].

A model of the formation of SiC-grain structure consisting of nuclei with a boundary layer on their surface is presented in [2]. The presence of the elements Y, Al and O in the boundary layer of silicon carbide grains was determined by metallographic methods. A detailed study of the mechanism of dissolution – recrystallization during liquid-phase sintering of silicon carbide with a sintering additive consisting of yttrium aluminum garnet is presented in [2, 3].

A similar model of the structure nucleus – boundary layer – intergrain phase is characteristic for many ceramic systems, which Si_3N_4/SiAlON, $BaTiO_3$-based solid alloys and carbonitrides with Co- and Ni-binder are [4, 5].

The formation of an amorphous boundary phase on silicon nitride grains was discovered during sintering of the composition Si_3N_4–MgO [6, 7]. The model developed for sintering of silicon nitride with oxide additives [8, 9] showed the formation of an amorphous film of the order of 1 – 2 nm thick on silicon nitride grains; this is a result of attractive (Van der Waals) forces acting between grains and repulsive (capillary) forces at the boundary of a grain and the oxide additive. Subsequently, it was shown that a SiAlON boundary layer forms on Si_3N_4 nuclei during sintering of Si_3N_4 with the addition of aluminum-nitrate garnet $3Y_2O_3 \cdot 5Al_2O_3$ [10, 11].

The present work is devoted to a more detailed study of the mechanism of liquid-phase sintering of the carbide LPSSiC and silicon nitride SSN with oxide sintering additives in the system Al_2O_3–Y_2O_3–MgO.

MATERIALS AND METHODS

The following powders were used: SiC (Volzhsk Abrasives Plant, Volzhsk), comminuted in a jet mill to particle size $d_{0.5} = 0.85$ μm; Si_3N_4, LS-12 grade (Berlin, Germany), obtained by furnace sintering, average particle diameter $d_{0.5} = 0.75$ μm (Table 1). The oxides Al_2O_3, Y_2O_3 and MgO were used as sintering additives; they were added in a strictly eutectic ratio in accordance with the phase diagram of the ternary system MgO–Y_2O_3–Al_2O_3 along the garnet–spinel section, which determines the melting temperature of the oxide phase — 1775°C [12]. The particle sizes in the pure-grade oxide powders were: Al_2O_3 — $d_{0.5} = 1.0$ μm; Y_2O_3 — $d_{0.5} = 1.0$ μm and MgO — $d_{0.5} = 0.6$ μm. The particle size distribution of the initial powders is presented in histograms

TABLE 1. Phase and Elemental Composition of Silicon Nitride Powder

Material	Composition of silicon nitride powder, %							
	α-Si_3N_4	β-Si_3N_4	Si_{bound}	N	Si_{free}	O	C	Fe
Si_3N_4	< 26.0	> 74.0	> 59.5	> 39.0	< 0.3	< 0.5	< 0.1	< 0.3

[1] Central Scientific-Research Institute of Metallurgy and Materials, JSC, St. Petersburg, Russia (e-mail: perevislov@mail.ru).

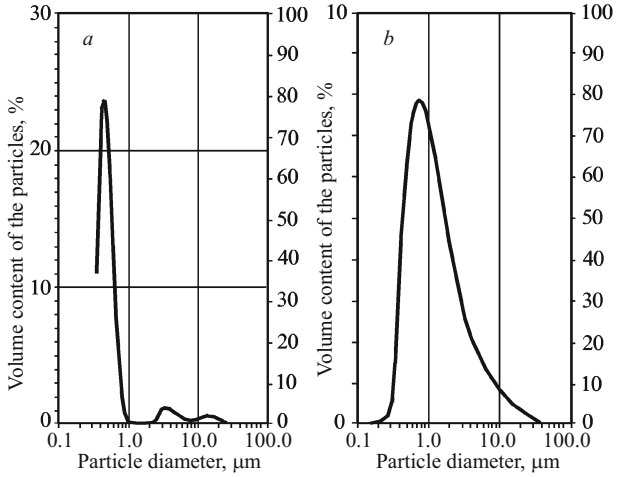

Fig. 1. Histograms of the particle size distribution: *a*) silicon carbide; *b*) silicon nitride.

(Fig. 1). The compositions and theoretical densities of the starting materials are presented in Table 2.

The starting powders taken in the required ratios (Table 2) were mixed in ethyl alcohol in a drum mixer. A 2% solution of organic binders was used as a plasticizing agent. The suspension was dried in a vacuum cabinet. The powder was granulated and samples for metallographic analysis were pressed from it by semi-dry molding. The samples were sintered at the following temperatures: LPSSiC at 1930°C with isothermal soaking for 1 h in a protective atmosphere, consisting of ultrapure argon, and SSN at 1780°C with isothermal soaking for 1 h in an ultrapure gas atmosphere.

The density of the sintered samples was determined analytically following GOST 20018–74. X-ray phase analysis was performed with a DRON-3M diffractometer using CuK α-radiation (λ = 1.54158 Å) and an Ni filter. The porosity was determined by studying the microstructure under an MIM-10 optical metallographic microscope with a VideoTest computer data analyzer. A Qwanta 200 electron microscope was used to determine the grain size and study the microstructure.

RESULTS

The microstructures of the LPSSiC- and SSN-materials (Fig. 2) are similar to the microstructure obtained in [1]. The structure of LPSSiC-material consists of homogenous grains

TABLE 2. Compositions of the Experimental Ceramic Materials

Composition No.	Component content, wt.%					Theoretical density, g/cm^3
	oxides			starting powders		
	Al_2O_3	Y_2O_3	MgO	SiC	Si_3N_4	
1	5.20	4.10	0.70	90	–	3.30
2	5.20	4.10	0.70	–	90	3.30

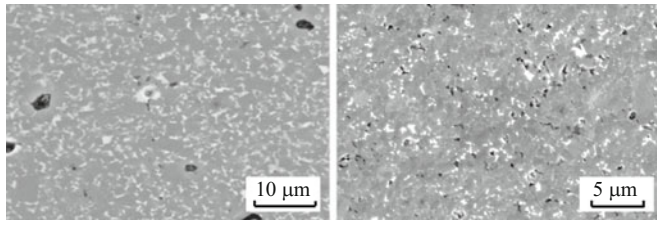

Fig. 2. Microstructure of LPSSiC- (*a*) and SSN-materials (*b*).

of size $D = 1 - 2$ μm (Fig. 2a) with an oxide binder uniformly distributed between SiC particles. The structure of the SSN-material is represented predominately of elongated grains of size $L \times D = (1 - 2) \times (0.2 - 0.5)$ μm and an oxide phase between them (Fig. 2*b*). The properties of LPSSiC- and SSN-materials are shown in Table 3.

According to the x-ray diffraction data for the LPSSiC-material (Fig. 3*a*) the primary crystalline phase is α-SiC and the secondary phase consists of yttrium aluminum garnet (YAG) oxides and magnesia spinel (MS), but small quantities of mutually miscible phases could exist. Analysis of SiC for the content of polytypes showed the presence of a large quantity of 6H–SiC before and after sintering (Table 4); this is confirmed by many studies where α-SiC and β-SiC powders were sintered with oxide additives [13, 14].

The β-SiC (3C-SiC polytype) present in the initial powder completely transforms in a $\beta \rightarrow \alpha$ phase transition into 4H and 6H polytypes of silicon carbide. In the SSN material the primary components are SiAlON, β-Si_3N_4 and the secondary components are the oxynitride β-Si_2N_2O and oxide phases YAG and MS (Fig. 3*b*).

A quantitative elemental x-ray phase analysis of LPSSiC (Fig. 4) revealed the presence of three regions in the material (elements content by weight): center of a carbide grain (nucleus) — 70.3% Si and 29.7% C, which corresponds to the composition of pure single-crystalline SiC; grain edge (boundary layer) — small quantities (to 1.5%) of Y, Al, Mg and O are present; the space between three carbide grains (inter-grain phase) corresponds to the content of practically pure oxide phases. The small amount of Si and C in the composition of the intergrain phase is due to either the dissolution of the oxide layer on the surface of SiC particles and the formation of a silicate oxide or very weak dissolution of silicon carbide in oxide, not exceeding the maximum solubility (Table 5). Si_3N_4 with oxide additives sinters according to a similar principle (Fig. 5, Table 6).

TABLE 3. Properties of the LPSSiC- and SSN-Materials

Material	Density ρ_{rel} (±0.2), g/cm^3	Porosity P (±0.2), %	Grain size, μm		Pore size, μm	
			max	min	max	min
LPSSiC	98.4	1.9	2.7	0.3	2.3	0.5
SSN	97.2	3.1	$L = 2.3$	$L = 0.2$	0.8	0.3

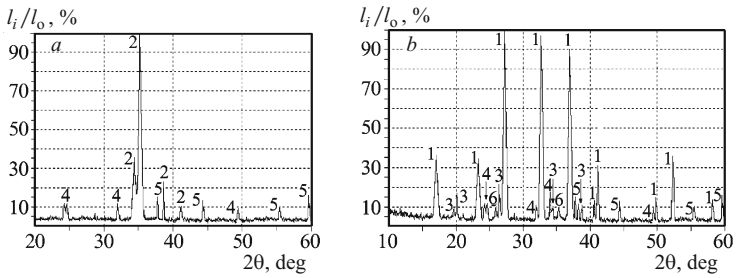

Fig. 3. X-ray phase diffraction patterns of sintered LPSSiC- (*a*) and SSN-materials (*b*): *1*) β-Si_3N_4; *2*) α-SiC; *3*) β-Si_2N_2O; *4*) $3Y_2O_3 \cdot 5Al_2O_3$; *5*) $MgO \cdot Al_2O_3$; *6*) SiAlON.

DISCUSSION

An important circumstance is that for full wetting of the SiC and Si_3N_4 grains by oxide melt the boundary layer on the surface of the primary grains grows uniformly in all directions. When two particles with no access to the oxide phase are in contact a boundary layer does not form at the contact locations.

During sintering the soaking time regulates the diffusion of Y, Al and Mg from the oxide melt into SiC grains. The amount of oxides has no effect on the thickness of the boundary layer on the grains.

For good wettability of the solid phase by a liquid (wetting angle close to 0°) the surface tension forces facilitate the rearrangement of the particles and subsequent densification of the material. Under the action of the capillary forces the liquid spreads over the surface of particles, wetting the space between the particles (pores), facilitating the rearrangement of the particles. Since in liquid-phase sintering of silicon carbide the amount of oxides introduced into the initial material is sufficient to fill the entire volume of the pores, the densification of the LPSSiC material proceeds in the following stages:

1) redistribution of the liquid under the action of capillary forces and restructuring of the solid particles by mutual slippage along grain boundaries;

2) densification of the material by means of dissolution – recrystallization; fine SiC particles with high curvature of the surface dissolve in the oxide melt, forming a solid solution;

3) the final stage of sintering, characterized by Ostwald grain growth [15]; when the melt becomes saturated to maximum solubility SiC precipitates onto the surfaces of the initial particles (nuclei) with low surface curvature in the form of a ring-shaped boundary layer.

TABLE 4. Volume Fractions of SiC Polytypes Before and After Sintering

SiC polytype	SiC content, vol.%	
	pre-sintering	post-sintering
3C	2.4	0.0
4H	4.6	5.3
6H	93.0	94.7

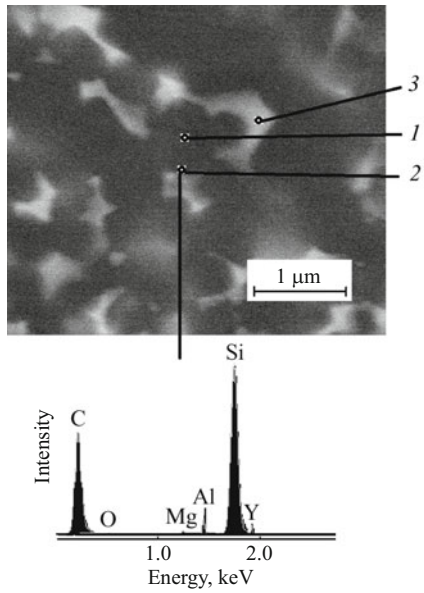

Fig. 4. Microstructure and elemental x-ray phase analysis of LPSSiC material: the numbers *1 – 3* refer to the sections studied (see Table 5).

The microstructure of the LPSSiC materials consists of 'SiC grains' (nuclei and boundary layer) and an intergrain oxide phase.

High solubility of the solid matter in the liquid phase is not necessary for high densification in the process of liquid-phase sintering. On the contrary, high solubility of the liquid in the solid phase must be avoided, since this will probably cause the material to swell and then fracture.

The structure of the SSN-material, just as LPSSiC, is represented by a model of a grain (nucleus and boundary layer) – the intergrain phase, but the sintering mechanism is somewhat different:

TABLE 5. Elemental Composition of LPSSiC-Material

Section No.	Elemental content of material, wt.%					
	Si *K*	C *K*	O *K*	Al *K*	Mg *K*	Y *L*
1	70.3	29.7	0	0	0	0
2	69.0	29.5	0.6	0.5	0.3	0.1
3	0.3	0.1	37.1	27.4	3.6	31.5

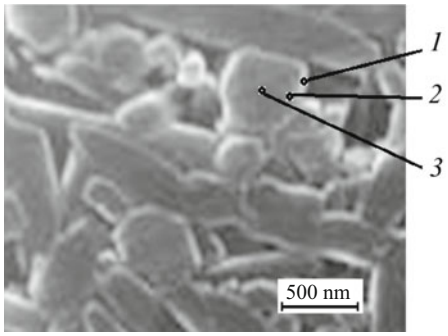

Fig. 5. Microstructure of an etched thin section of SSN-material: the numbers *1 – 3* refer to the sections studied (see Table 6).

– interaction of Si_3N_2 particles with the oxides at the locations of contact with the formation of the SiAlON phase;

– softening of the oxides and their saturation by the nitride phase owing to the dissolution of the fine Si_3N_4 particle in the oxide;

– growth of an SiAlON layer on the surface of the large silicon nitride particles;

– maximum densification owing to the redistribution of the remaining oxide melt in the intergrain spaces (pores).

As a result of the $\alpha \rightarrow \beta$ phase transition a structure including elongated 'Si_3N_4 grains' (Si_3N_4 nuclei with an SiAlON boundary layer) forms in the material. The elongated grains grow in a direction predominately perpendicular to the force of formation of the blanks.

The thickness of the SiAlON layer is independent of the amount of oxide components in the material. The Si_3N_4 grains with a 'SiAlON boundary layer' no longer dissolve in the oxide melt, and saturation of the latter by the nitride phase ceases. As a rule, the SiAlON layer occupies 15 – 25 vol.% of a 'Si_3N_4 grain' formed (see Fig. 5).

CONCLUSIONS

The mechanism of sintering was studied and the formation of structure in the liquid-phase-sintered silicon carbide and sintered silicon nitride was investigated. The microstructure of the LPSSiC-materials consists of 'SiC grains' (nucleus and boundary layer) and an intergrain oxide phase. The structure of the SSN-material is also represented by the model nucleus (Si_3N_4 grain) – boundary layer (SiAlON) – intergrain phase. The data obtained on the liquid-phase sintering of SiC and Si_3N_4 make possible to model the properties of the LPSSiC- and SSN-materials obtained.

TABLE 6. Elemental Composition of SSN-Material

Section No.	Si *K*	N *K*	O *K*	Al *K*	Mg *K*	Y *L*
1	32.6	24.8	16.2	22.8	0.2	3.4
2	59.3	35.8	4.9	0	0	0
3	60.5	39.5	0	0	0	0

REFERENCES

1. S. N. Perevislov, V. D. Chupov, and M. V. Tomkovich, "Effect of activating yttrium aluminum garnet and magnesia spinel additives on the compactibility and mechanical properties of SiC ceramic," *Vopr. Materialoved.*, **65**(1), 123 – 129 (2011).
2. L. S. Sigl and H. J. Kleebe, "Core/rim structure of liquid-phase-sintered silicon carbide," *J. Am. Ceram. Soc.*, **76**(3), 773 – 776 (1993).
3. H. Xu, T. Bhatia, S. A. Deshpande, et al., "Microstructural evolution in liquid-phase-sintered SiC. Part I. Effect of starting powder," *J. Am. Ceram. Soc.*, **84**(7), 1578 – 1584 (2001).
4. O. Rudiger and H. E. Exner, "Application of Basic Research to the development of hard metals," *Powder Metdi. Fnc.*, No. 8, 7 – 13 (1976).
5. T. Schmitt, M. Schreiner, P. Ettmayer, et al., "On solution reprecipitation processes during liquid phase sintering of WCCo," *Refract. Hard. Mater.*, No. 3, 78 – 83 (1983).
6. E. Mirica, P. Mukundhan, H. Du, and S. W. Lee, "Effects of MgO additive on the oxidation kinetics and oxide characteristics of Si_3N_4," in: *101-st Annual Meeting and Exposition 'Setting the Pace for the Next Century', Indianapolis, Indiana, 25 – 28 Apr. 1999*, Indianapolis (1999), p. 362.
7. W. Linjun, Ch. Kaixian, and S. Rongguo, "Effect of Al and Si on the strength and microstructure of composite MgO–Si_3N_4," *Naihuo Cailiao*, **38**(6), pp. 420 – 422 (2004).
8. D. R. Clarke, "On the equilibrium thickness of intergranular glass phases in ceramic materials," *J. Am. Ceram. Soc.*, **70**(1), pp. 15 – 22 (1987).
9. D. R. Clarke, T. M. Shaw, A. P. Philipse, and R. G. Horn, "Possible electrical double-layer contribution to the equilibrium thickness of intergranular glass gilms in polycrystalline ceramics," *J. Am. Ceram. Soc.*, **76**(5), pp. 1201 – 1204 (1993).
10. M. Mamoru, H. Naoto, N. Toshiyuki, and X. Rong-Ju, "Microstructure control in silicon nitride ceramics," *Nippon Seramikkusu Kyokai Gakujutsu Ronbunshi*, **114**(1335), pp. 867 – 872 (2006).
11. C. Santos, K. Strecker, S. Ribeiro, J. V. C. de Souza, et al., "α-SiAlON ceramics with elongated grain morphology using an alternative sintering additive," *Mater. Lett.*, **58**(11), 1792 – 1796 (2004).
12. S. N. Perevislov, V. D. Chupov, S. S. Ordan'yan, and M. V. Tomkovich, "Obtaining high-density silicon carbide materials by liquid-phase sintering in the system SiC–Al_2O_3–Y_2O_3–MgO," *Ogneup. Tekh. Keram.*, No. 4 – 5, 26 – 32 (2011).
13. A. Balbo, D. Sciti, and A. Bellosi, "Pressureless liquid phase sintering of silicon carbide in function of the powders characteristics," *Int. J. Appl. Ceram.*, **22**(4), 33 – 37 (2004).
14. Y.-I. Lee, Y.-W. Kim, and M. Mitomo, "Microstructure stability of fine-grained silicon carbide ceramics during annealing," *J. Mater. Sci.*, **39**(11), 3613 – 3617 (2004).
15. R. M. German, *Liquid Phase Sintering*, Plenum Press, N.Y. (1985).